Journal of Machine Engineering, 2026, Vol. 26
ISSN 1895-7595 (Print) ISSN 2391-8071 (Online)

Received*: 16 February 2026* / Accepted: *30 April 2026* / Published online: *18 May 2026*

3D printing,
optimization,
bio-inspired structures

Tien-Dat HOANG[1], Ha Linh NGO[1],
Quy Tho NHU[1], Van Dam VU[2*]

COMPARATIVE MULTI-CRITERIA DECISION MAKING ANALYSIS FOR OPTIMIZING MECHANICAL PERFORMANCE OF BIO-INSPIRED STRUCTURES FABRICATED BY FUSED DEPOSITION MODELLING

Three-dimensional (3D) printing via fused deposition modelling (FDM) enables the fabrication of complex bio-inspired structures with high design flexibility; however, achieving an optimal balance among mechanical performance indicators remains challenging. This study proposes a comparative multi-criteria decision-making (MCDM) framework for optimizing the performance of FDM-fabricated bio-inspired structures, including Gyroid (G), I-graph-wrapped package (IWP), Fischer–Koch–S (FKS), and Primitive–Gyroid–Modified–Y (PMY). Eight specimens manufactured using polylactic acid (PLA) and PLA reinforced with short carbon fibers (PLA–CF) were experimentally evaluated under compression to determine mass, deformation, load-bearing capacity, and elastic modulus. Objective criterion weights were determined using the MEREC method, and three MCDM techniques, SAW, TOPSIS, and EAMR were employed for performance ranking and comparison. The results consistently identify PMY printed with PLA–CF as the optimal design across all methods, demonstrating the robustness and reliability of the proposed framework. Overall, the optimal structure exhibits a favourable combination of low mass, high load capacity, minimal deformation, and superior elastic modulus. This study provides a systematic and experimentally validated approach for multi-objective mechanical optimization of bio-inspired structures in additive manufacturing.

1. INTRODUCTION

Additive manufacturing (AM), commonly referred to as three-dimensional (3D) printing, has emerged as a transformative manufacturing paradigm due to its capability to fabricate geometrically complex structures that are difficult or impossible to achieve using conventional subtractive methods [1]. Among various AM technologies, fused deposition modelling (FDM) remains one of the most widely adopted processes owing to its low cost, material versatility, and suitability for rapid prototyping and functional part fabrication [2, 3]. As a result, FDM has been extensively applied in aerospace, biomedical engineering,

[1] School of Mechanical and Automotive Engineering, Hanoi University of Industry, Vietnam
[2] Department of Facilities Management, Thai Nguyen University, Vietnam
[*] E-mail: vudam@tnu.edu.vn
https://doi.org/10.36897/jme/221265

lightweight structural components, and energy-absorbing systems, where structural efficiency and mechanical reliability are critical requirements [4].

In recent years, increasing attention has been directed toward bio-inspired structural designs, particularly triply periodic minimal surface (TPMS) and lattice-based architectures, due to their exceptional strength-to-weight ratio, deformation control, and energy absorption characteristics [5, 6]. Structures such as Gyroid, Fischer–Koch–S, and I-graph-wrapped package geometries have demonstrated superior mechanical performance compared to conventional solid or honeycomb designs, especially under compressive loading conditions [7, 8]. These bio-inspired geometries enable efficient material distribution and load transfer mechanisms, making them attractive for lightweight and load-bearing applications in additive manufacturing [9, 10].

Despite these advantages, the performance of FDM-printed bio-inspired structures is strongly influenced by multiple interacting factors, including geometry, material composition, fiber reinforcement, and internal architecture [11, 12]. Polymer composites, such as polylactic acid reinforced with short carbon fibers (PLA–CF), have been increasingly adopted to enhance stiffness and load-bearing capacity of FDM-printed parts [13]. However, the heterogeneous microstructure introduced by fiber reinforcement, combined with layer-by-layer deposition and anisotropy inherent to FDM, significantly complicates the accurate prediction and optimization of mechanical properties.

Most existing studies on FDM-printed bio-inspired structures focus on single-objective optimization, such as maximizing strength or minimizing mass, or on parametric studies involving process parameters (e.g., layer thickness, raster angle, and printing speed) [14, 15]. While these approaches provide valuable insights, real-world engineering applications typically require the simultaneous satisfaction of multiple conflicting performance criteria, including low mass, high load-bearing capacity, minimal deformation, and high elastic modulus. Consequently, single-objective optimization strategies are insufficient to capture the trade-offs inherent in practical structural design problems.

Multi-criteria decision-making (MCDM) methods offer a systematic framework for evaluating and ranking alternative design solutions when multiple, often conflicting, criteria must be considered simultaneously [16]. Techniques such as the simple additive weighting (SAW) [17], technique for order preference by similarity to ideal solution (TOPSIS) [18], and evaluation by area-based method of ranking (EAMR) [19] have been successfully applied in manufacturing process optimization, material selection, and structural design. However, a major limitation in many MCDM-based studies lies in the subjective assignment of criterion weights, which can significantly influence ranking outcomes and reduce the objectivity of the optimization process. Although classical MCDM methods such as SAW, and TOPSIS have been widely used in manufacturing and material selection, their application to architected additive-manufactured structures remains limited and often method-dependent. Most existing studies rely on a single technique with subjectively assigned weights, and the robustness of ranking results is rarely examined, particularly for complex TPMS-based geometries exhibiting nonlinear mechanical behaviour.

To address this limitation, the method based on the removal effects of criteria (MEREC) has recently been introduced as an objective weighting approach that quantifies the influence of each criterion on the overall decision outcome [20]. By systematically evaluating the effect

of removing individual criteria, MEREC provides an unbiased and data-driven mechanism for weight determination, thereby enhancing the reliability of MCDM results. Nevertheless, the application of MEREC in the optimization of bio-inspired FDM-printed structures remains limited in the existing literature. Therefore, the primary objective of this study is to develop a comparative and experimentally validated MCDM framework for optimizing the mechanical performance of bio-inspired structures fabricated by FDM. Four representative bio-inspired geometries, Gyroid (G), I-graph-wrapped package (IWP), Fischer–Koch–S (FKS), and Primitive–Gyroid–Modified–Y (PMY), were designed and fabricated using PLA and PLA–CF materials. Compression experiments were conducted to evaluate mass, deformation, load-bearing capacity, and elastic modulus. Criterion weights were objectively determined using the MEREC method, and three MCDM techniques (SAW, TOPSIS, and EAMR) were systematically compared to identify the optimal structural configuration. The results demonstrate strong consistency among different MCDM methods and highlight the effectiveness of the proposed framework for multi-objective mechanical optimization of bio-inspired FDM-printed structures.

2. THEORETICAL BACKGROUND

2.1. GEOMETRICAL AND MATHEMATICAL FORMULATION OF BIO-INSPIRED STRUCTURES

In this study, the bio-inspired structures were modeled using implicit level-set equations, which are widely employed to describe triply periodic minimal surface (TPMS) and TPMS-derived architectures. In this formulation, each structure is defined by a scalar function, and the solid–void interface is obtained by extracting an iso-surface at a prescribed level-set constant:

$$\phi(x, y, z) = c \tag{1}$$

The parameter c controls the relative density of the structure, while the spatial periodicity is governed by the unit-cell size a. For convenience, the spatial coordinates are normalized as:

$$X = \frac{2\pi x}{a}, Y = \frac{2\pi y}{a}, Z = \frac{2\pi z}{a} \tag{2}$$

The Gyroid (G) structure is represented by the following implicit equation:

$$\phi_G(X, Y, Z) = \sin X \cos Y + \sin Y \cos Z + \sin Z \cos X = c \tag{3}$$

which generates a continuous and non-self-intersecting surface characterized by smooth curvature and isotropic connectivity. This geometry is well known for its high stiffness-to-weight ratio and uniform stress distribution under compressive loading.

The I-graph-wrapped package (IWP) structure is described by a higher-order trigonometric formulation:

$$\phi_{IWP}(X,Y,Z) = 2(\cos X \cos Y + \cos Y \cos Z + \cos Z \cos X) - (\cos 2X + \cos 2Y + \cos 2Z) = c \quad (4)$$

This formulation introduces more complex internal connectivity and enhanced load-transfer pathways, leading to improved load-bearing capability compared to simpler TPMS geometries.

The Fischer–Koch–S (FKS) structure is generated using a mixed trigonometric expression involving first- and second-order periodic components:

$$\phi_{FKS}(X,Y,Z) = \cos(2X)\sin \mathrm{Y}\cos Z + \cos \mathrm{X}\cos(2Y)\sin Z + \sin X \cos Y \cos(2Z) = c \quad (5)$$

Due to its asymmetric connectivity, the FKS structure exhibits tailored stiffness and anisotropic deformation characteristics, which can be advantageous for direction-dependent mechanical applications.

To further enhance performance, a hybrid Primitive–Gyroid–Modified–Y (PMY) architecture was constructed by blending multiple TPMS level-set functions. The Primitive surface is defined as:

$$\phi_P(X,Y,Z) = \cos X + \cos Y + \cos Z \quad (6)$$

while the Gyroid function ϕ_G is given above. A modified Y-type function ϕ_Y was incorporated to enrich structural connectivity. The resulting PMY structure is expressed as:

$$\phi_{PMY}(X,Y,Z) = w_P\phi_P(X,Y,Z) + w_G\phi_G(X,Y,Z) + w_Y\phi_Y(X,Y,Z) = c \quad (7)$$

where w_P, w_G, and w_Y are non-negative weighting coefficients satisfying $w_P + w_G + w_Y = 1$. By adjusting these weighting parameters and the level-set constant c, the mechanical behavior of the PMY structure can be finely tuned while preserving geometric periodicity and manufacturability.

Overall, the implicit level-set representation provides a mathematically robust and flexible framework for generating complex bio-inspired geometries. This approach ensures geometric continuity, enables parametric control of relative density, and facilitates seamless integration with numerical simulation, topology optimization, and fused deposition FDM fabrication processes.

2.2. MULTI-CRITERIA DECISION-MAKING METHODS

In this study, the optimization of mechanical performance for bio-inspired FDM fabricated structures involves multiple, often conflicting criteria. To address this problem, several MCDM techniques were employed to evaluate and rank alternative structural designs in a systematic and quantitative manner.

An MCDM problem can be represented by a decision matrix:

$$\mathbf{X} = [x_{ij}]_{m\times n} \quad (8)$$

where m denotes the number of alternatives (specimens), n is the number of evaluation criteria, and x_{ij} represents the performance value of alternative i with respect to criterion j.

The criteria are classified as benefit-type criteria (larger values are preferable), load-bearing capacity and elastic modulus. Cost type criteria (smaller values are preferable), e.g., mass and deformation, and to eliminate dimensional inconsistency, the decision matrix is first normalized.

2.2.1. OBJECTIVE WEIGHT DETERMINATION USING MEREC

The Method based on the Removal Effects of Criteria is used to objectively determine criterion weights based solely on experimental data.

Step 1: Normalization

For benefit-type criteria:

$$r_{ij} = \frac{x_{ij}}{\max\limits_{i} x_{ij}} \tag{9}$$

For cost-type criteria:

$$r_{ij} = \frac{\min\limits_{i} x_{ij}}{x_{ij}} \tag{10}$$

Step 2: Overall performance of alternatives

$$S_i = \sum_{j=1}^{n} r_{ij} \tag{11}$$

Step 3: Performance with criterion removal

$$S_{ij}^{(-\mathrm{j})} = \sum_{\substack{k=1 \\ k \neq j}}^{n} r_{ik} \tag{12}$$

Step 4: Removal effect of each criterion

$$E_j = \sum_{i=1}^{m} | S_i - S_{ij}^{(-j)} | \tag{13}$$

Step 5: Criterion weights

$$w_j = \frac{E_j}{\sum_{j=1}^{n} E_j} \tag{14}$$

where w_j denotes the objective weight of criterion j.

2.2.2. SIMPLE ADDITIVE WEIGHTING (SAW) METHOD

The SAW method aggregates weighted normalized criteria into a single performance score.

Step 1: Normalization

The normalized matrix r_{ij} follows the same formulation as in the MEREC method.
Step 2: Weighted summation

$$V_i = \sum_{j=1}^{n} w_j r_{ij} \tag{15}$$

where V_i is the overall score of alternative i.
The alternative with the highest V_i is considered optimal.

2.2.3. TECHNIQUE FOR ORDER PREFERENCE BY SIMILARITY TO IDEAL SOLUTION (TOPSIS)

TOPSIS ranks alternatives based on their distances to an ideal and an anti-ideal solution.
Step 1: Vector normalization

$$r_{ij} = \frac{x_{ij}}{\sqrt{\sum_{i=1}^{m} x_{ij}^2}} \tag{16}$$

Step 2: Weighted normalized matrix

$$v_{ij} = w_j r_{ij} \tag{17}$$

Step 3: Ideal and negative-ideal solutions

$$A^+ = \{\max\ v_{ij} \mid j \in J_b; \min\ v_{ij} \mid j \in J_c\} \tag{18}$$

$$A^- = \{\min v_{ij} \mid j \in J_b; \max v_{ij} \mid j \in J_c\}$$

where J_b and J_c represent benefit and cost criteria, respectively.
Step 4: Separation measures

$$D_i^+ = \sqrt{\sum_{j=1}^{n} (v_{ij} - A_j^+)^2}, D_i^- = \sqrt{\sum_{j=1}^{n} (v_{ij} - A_j^-)^2} \tag{19}$$

Step 5: Closeness coefficient

$$C_i = \frac{D_i^-}{D_i^+ + D_i^-} \tag{20}$$

The alternative with the highest C_i is preferred.

2.2.4. EVALUATION BY AREA-BASED METHOD OF RANKING (EAMR)

The EAMR method evaluates alternatives based on weighted normalized scores.
Step 1: Weighted normalized values

$$p_{ij} = w_j r_{ij} \tag{21}$$

Step 2: Score computation

$$S_i = \sum_{j \in J_b} p_{ij} - \sum_{j \in J_c} p_{ij} \tag{22}$$

The alternative with the maximum S_i is ranked highest.

By integrating objective criterion weighting via MEREC with three complementary MCDM ranking techniques, this study establishes a robust and reliable framework for the optimization. The consistency of ranking results across different MCDM methods provides strong evidence for the stability of the identified optimal bio-inspired structure.

3. EXPERIMENTAL AND RESULTS

3.1. DESIGN AND FABRICATION OF BIO-INSPIRED STRUCTURES

Four representative bio-inspired unit-cell geometries G, IWP, FKS, and PMY were selected for experimental investigation due to their distinct topological characteristics and mechanical potential. All structures were generated using the implicit level-set equations described in Section 2, ensuring geometric continuity and periodicity. Each unit cell was uniformly scaled and assembled into a solid specimen with identical external dimensions to eliminate size effects and ensure fair comparison among different geometries. The level-set constant *c* was adjusted to achieve comparable relative densities across all specimens. This approach allows the mechanical response to be primarily governed by the internal architecture rather than by differences in overall volume or mass. In this paper, each model was built with 50% porosity as showed in Fig. 1.

Two types of filament materials were employed in this study pure PLA and polylactic acid reinforced with PLA–CF. The PLA–CF filament was selected to investigate the influence of fiber reinforcement on the mechanical performance of bio-inspired structures fabricated by FDM. All specimens were fabricated using the same FDM system under identical printing conditions to minimize process-induced variability. The nozzle diameter, layer thickness, raster pattern, printing speed, and extrusion temperature were kept constant for all prints as given in Table 1. The build orientation was fixed to ensure consistent layer stacking and interlayer bonding characteristics. No post-processing treatments were applied after printing. For each geometry and material combination, three specimens were fabricated to evaluate printing quality and dimensional consistency. Among these printed samples, the specimen with the best dimensional accuracy and without visible printing defects was selected for compression testing.

Due to limitations in fabrication time and material consumption, one compression test was performed for each selected specimen. Therefore, the reported mechanical values should be interpreted as representative experimental results rather than statistically averaged data. Future work will include repeated mechanical testing with a larger sample size to report mean values, standard deviations, and confidence intervals. With each bio-inspired geometry after several testing, specimens were printed using both PLA and PLA–CF materials, resulting in a total of eight samples for experimental evaluation as in Fig. 2.

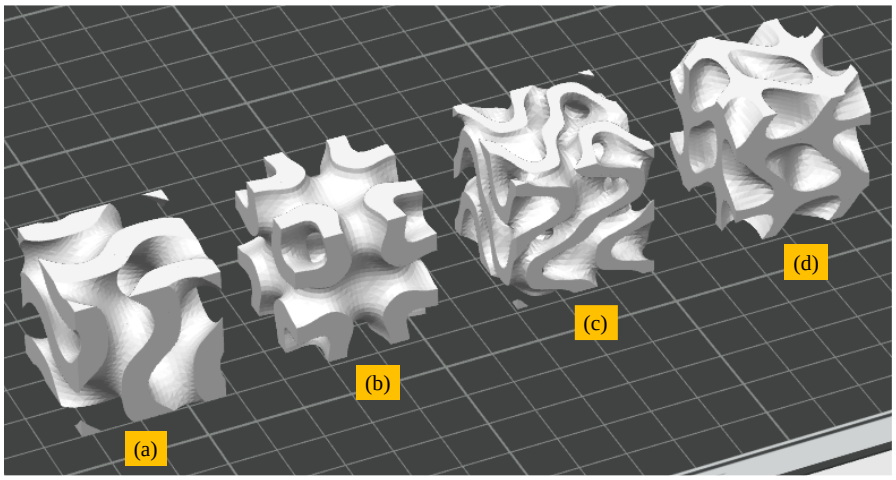

Fig. 1. Four TPMS structures: (a). G, (b). P, (c). FKS, (d). PMY (size 20 x 20 x 20 mm)

Table 1. Printing process parameters

Temperature (^{0}C)	Printing speed (mm/s)	Layer thickness (mm)	Printing Infill (%)	Raster pattern	Nozzle diameter (mm)
00000000235	60	0.15	100	Line	0.4

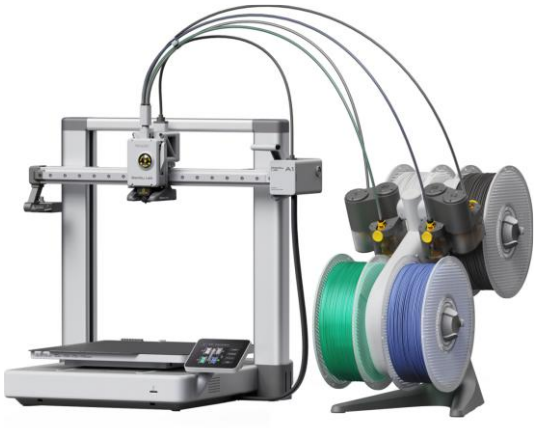

(a). Bamboo Lab A1 printer

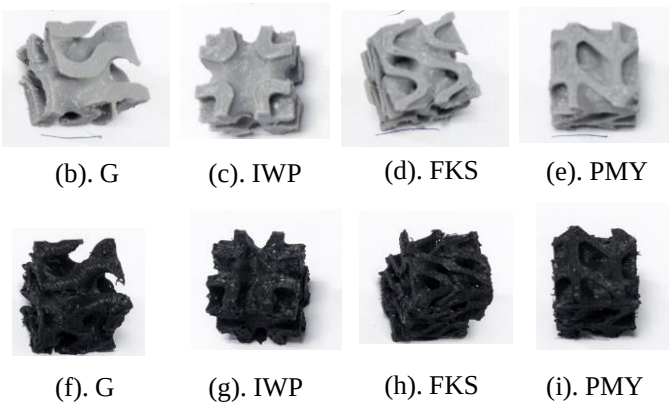

(b). G (c). IWP (d). FKS (e). PMY

(f). G (g). IWP (h). FKS (i). PMY

Fig. 2. Printed specimens: PLA material (b), (c), (d), (e); PLA-CF material (f), (g), (h), (i)

3.2. COMPRESSION TESTING SETUP

Uniaxial compression tests were conducted to evaluate the mechanical performance of the printed specimens in Instron 3382A, USA. Each specimen was placed centrally between two parallel platens of a universal testing machine to ensure uniform load distribution during testing as in Fig. 3. The compression load was applied under displacement control at a constant crosshead speed until structural failure occurred. During testing, force-displacement data were continuously recorded. The deformation behaviour was monitored throughout the loading process to capture the elastic and post-elastic response of each structure. To minimize experimental error, all tests were conducted under ambient laboratory conditions, and care was taken to ensure proper alignment of specimens before loading.

Figure 4 shows the microstructure of the 3D-printed PLA–CF specimen observed using a WHX-7100 digital microscope (Keyence). Short carbon fibers are clearly embedded in the PLA matrix with a relatively uniform spatial distribution, and no obvious fiber agglomeration or large fiber bundles are detected. Most fibers are oriented along the material flow direction during extrusion, while some misaligned fibers provide a three-dimensional reinforcement network. The measured fiber lengths are on the order of a few hundred micrometers (approximately 200–300 μm), which is consistent with short-carbon-fiber reinforcement typically used in FDM. This microstructural configuration is expected to enhance stress transfer and improve the stiffness of the bio-inspired structures printed with PLA–CF.

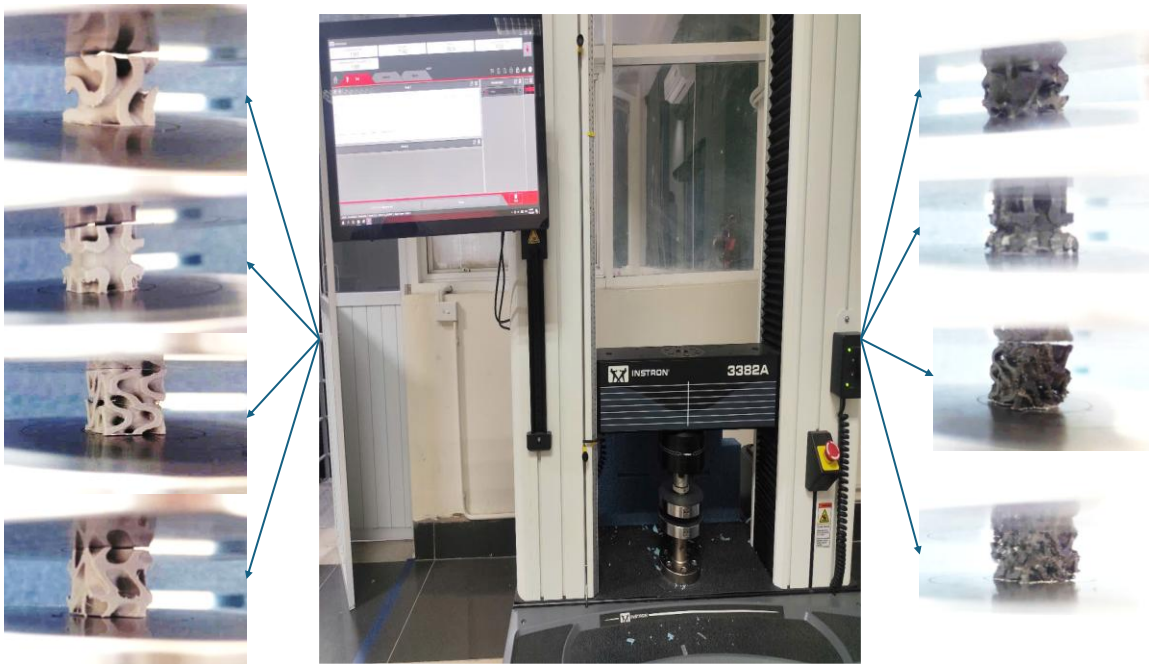

(a). PLA specimens (b). Instron 3382A compress equipment system (c). PLA-CF specimens

Fig. 3. Compress testing for eight specimens

Figure 5 illustrates the representative compressive stress–strain curves of the four bio-inspired architectures manufactured from PLA and PLA–CF. All specimens exhibit an initial linear elastic regime followed by a clear peak stress and subsequent softening, which is typical of cellular and lattice structures under compression. For each geometry, the PLA–CF structures (solid lines) display a steeper initial slope and noticeably higher peak stresses than their neat-PLA counterparts (dashed lines), confirming the stiffening and strengthening effect of short carbon-fiber reinforcement. Among the PLA–CF specimens, the PMY-CF structure achieves the highest compressive stress level and maintains a relatively high stress plateau over a wide strain range, indicating superior load-bearing capacity and energy absorption capability. In contrast, the neat-PLA TPMS structures show lower peak stresses and more pronounced post-peak stress decay, highlighting the beneficial role of the PLA–CF composite in improving the performance of the bio-inspired FDM-printed lattices. The compressive deformation of TPMS-based structures follows three stages. The deformation behaviour is strongly influenced by structural topology. Geometries with higher connectivity

and continuous curvature, such as PMY, promote more uniform stress distribution, reduce stress concentration, and delay structural instability, resulting in a more stable plateau region. Material and geometry interaction plays a key role in mechanical performance. The incorporation of short carbon fibers in PLA–CF enhances stiffness and stress transfer, while the TPMS architecture governs load paths and collapse mechanisms. This combination leads to improved load-bearing capacity, reduced deformation, and enhanced energy absorption compared to neat PLA structures. In general, the mechanical response is governed by the coupled effect of material properties and structural geometry, which determines stress redistribution efficiency and deformation stability under compression.

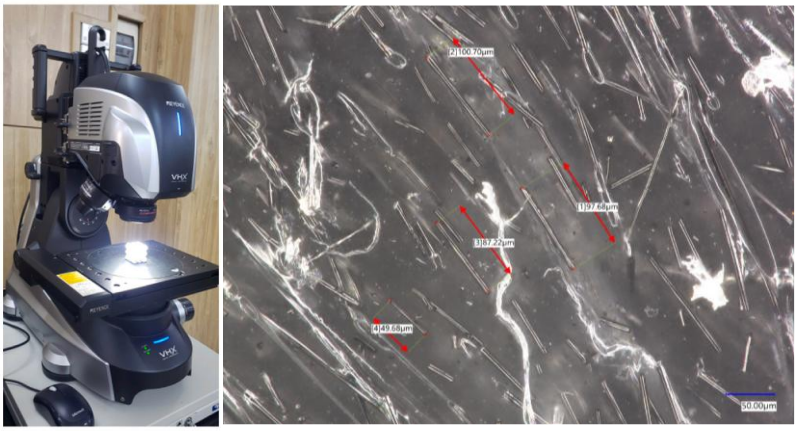

(a). VHX 7100, Keyence (b). Microstructure of PLA-CF specimen

Fig. 4. Microstructure of PLA-CF specimen

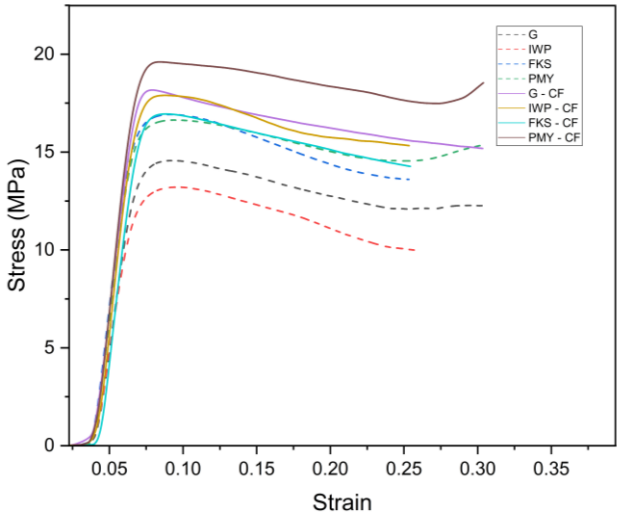

Fig. 5. Stress – strain curve of eight compressed specimens

In addition to the primary mechanical criteria, additional performance indicators were introduced to provide a more comprehensive evaluation of structural efficiency. The energy absorption (EA) was calculated as the area under the stress–strain curve up to the densification strain, defined as Eq. (23):

$$EA = \int_0^{\varepsilon} \sigma(\varepsilon) d\varepsilon \tag{23}$$

The energy absorption (EA) of each specimen was calculated by integrating the area under the stress–strain curve using numerical integration. The results are collected in Table 2. Overall, the incorporation of short carbon fibers results in a significant improvement in energy absorption, ranging from approximately 20% to 36% depending on the structural geometry.

Table 2. Energy absorption of each specimen

Specimen	IWP–CF	PMY–CF	FKS–CF	G–CF	IWP	PMY	FKS	G
EA (MJ/m³)	3.31	4.57	3.12	4.10	2.42	3.84	3.11	3.25

4. COMPARATIVE MULTI-CRITERIA DECISION-MAKING (MCDM)

The experimentally obtained values of mass, deformation, load-bearing capacity, and elastic modulus for each specimen were organized into a decision matrix. These four criteria were selected to represent both lightweight design requirements (mass and deformation) and mechanical robustness (load capacity and elastic modulus). Prior to MCDM evaluation, the criteria were classified as cost-type (mass and deformation) and benefit-type (load-bearing capacity and elastic modulus). Objective criterion weights were subsequently determined using the MEREC method, and the weighted decision matrix served as the basis for performance ranking using SAW, TOPSIS, and EAMR methods.

Based on the experimentally obtained mechanical properties from Fig. 5, a multi-objective optimization problem was formulated by simultaneously considering four criteria: deformation, mass, load-bearing capacity, and elastic modulus. Among these criteria, deformation and mass were treated as cost-type criteria, whereas load-bearing capacity and elastic modulus were classified as benefit-type criteria. The corresponding decision matrix is presented in Table 3. The specimens are indexed from 1 to 8, corresponding to IWP–CF, PMY–CF, FKS–CF, G–CF, IWP, PMY, FKS, G, respectively.

4.1. OBJECTIVE WEIGHT DETERMINATION USING THE MEREC METHOD

The MEREC method was employed to objectively determine the relative importance of each criterion, thereby eliminating subjective bias in the weighting process. The normalized decision matrix obtained using the MEREC normalization procedure is shown in Table 4. Subsequently, the overall performance of each specimen S_i and the performance values obtained after removing individual criteria S'_{ij} were calculated (Table 5).

The removal effect values E_j and the corresponding criterion weights w_j, summarized in Table 6, reveal a clear hierarchy among the considered criteria. The load-bearing capacity exhibits the highest weight ($w_F = 0.4873$), indicating that it is the most influential criterion in the overall mechanical optimization. This is followed by the elastic modulus

($w_E = 0.3105$), highlighting the importance of structural stiffness. In contrast, deformation ($w_\varepsilon = 0.1367$) and mass ($w_m = 0.0656$) play comparatively smaller roles in the decision-making process. These results are consistent with practical engineering requirements, where load-carrying capability and stiffness are often prioritized over lightweight considerations for load-bearing structures.

Table 3. Decision matrix

Specimen	Deformation	Mass (g)	Load (kN)	Elastic modulus (MPa)
1	0.253	5.19	15.33	676.88
2	0.303	5.03	18.54	707.26
3	0.254	5.13	14.27	633.79
4	0.303	5.30	15.18	641.43
5	0.257	5.04	9.99	482.96
6	0.301	4.86	15.34	609.43
7	0.253	4.88	13.61	610.71
8	0.304	5.01	12.26	533.04

By following the steps described in the theoretical framework, the MEREC method is applied to obtain the normalized values.

Table 4. Normalized values using the MEREC method

Specimen	Deformation	Mass	Load	Elastic modulus
1	0.8337	0.9792	0.6522	0.7135
2	0.9995	0.9491	0.5392	0.6829
3	0.8362	0.9679	0.7005	0.7620
4	0.9978	1.0000	0.6584	0.7529
5	0.8458	0.9509	1.0000	1.0000
6	0.9930	0.9170	0.6517	0.7925
7	0.8330	0.9208	0.7347	0.7908
8	1.0000	0.9434	0.8148	0.9060

The overall efficiency of the projects S_i, as well as the performance of the alternatives S'_{ij}, were determined and are presented in Table 5.

Table 5. Values S_i and S'_{ij} using the MEREC method

Specimen	S_i	S'_{ij}			
		Deformation	Mass	Load	Elastic modulus
1	0.2358	0.1956	0.2317	0.1306	0.1668
2	0.2322	0.2261	0.2218	0.1098	0.1536
3	0.1715	0.1411	0.1646	0.1058	0.1126
4	0.1813	0.1813	0.1813	0.0685	0.1203
5	0.0522	0.0125	0.0402	0.0522	0.0522
6	0.1730	0.1677	0.1547	0.0826	0.1229
7	0.1778	0.1418	0.1603	0.1147	0.1274
8	0.1067	0.0926	0.0936	0.0534	0.0843

The absolute values E_j and the weights for the criteria w_j are calculated, as presented in Table 6.

Table 6. Values E_j and w_j using the MEREC method

	Deformation	Mass	Load	Elastic modulus
E_j	0.1719	0.0825	0.6128	0.3905
w_j	0.1367	0.0656	0.4873	0.3105

4.2. SAW METHOD RESULTS

Using the criterion weights obtained from the MEREC method, the Simple Additive Weighting approach was applied to rank the eight specimens. The resulting priority values V_i and rankings are presented in Table 7. Specimen 2 achieved the highest SAW score, followed by Specimen 1 and Specimen 6. Conversely, Specimen 5 ranked lowest due to its relatively low load-bearing capacity and elastic modulus. The SAW results indicate that Specimen 2 provides the most balanced mechanical performance when all criteria are considered simultaneously.

Table 7. Values V_i and ranking of alternatives using the SAW method

Specimen	Vi	Rank
1	0.947011	2
2	0.976523	1
3	0.837917	5
4	0.908173	3
5	0.679675	8
6	0.859029	4
7	0.830887	6
8	0.760305	7

4.3. TOPSIS METHOD RESULTS

The TOPSIS method was subsequently employed to evaluate the relative closeness of each specimen to the ideal solution. The calculated distances to the positive ideal solution (S_i^+), negative ideal solution (S_i^-), and the corresponding closeness coefficients (C_i^*) are summarized in Table 8.

Specimen 2 again demonstrates the highest closeness coefficient, indicating that it is closest to the ideal mechanical performance among all alternatives. Specimens 1 and 6 rank second and third, respectively, while Specimen 5 exhibits the poorest performance. The consistency between the SAW and TOPSIS rankings further supports the robustness of Specimen 2 as the optimal design.

Table 8. Values S_i^+, S_i^-, C_i^* and ranking of alternatives using the TOPSIS method

Specimen	S_i^+	S_i^-	C_i^*	Rank
1	0.0171	0.0847	0.832144	2
2	0.0066	0.1008	0.938667	1
3	0.0529	0.0498	0.485306	5
4	0.0202	0.0834	0.805201	3
5	0.1008	0.0080	0.073486	8
6	0.0378	0.0639	0.628401	4
7	0.0555	0.0466	0.456823	6
8	0.0695	0.0320	0.31536	7

4.4. EAMR METHOD RESULTS

The Evaluation by Area-Based Method of Ranking (EAMR) was also applied to further validate the ranking results. As shown in Table 9, Specimen 2 consistently achieves the highest ranking, followed by Specimen 1 and Specimen 6. Since all criteria have been normalized into benefit-type values in Table 3 (higher is better), EAMR is applied directly to the weighted normalized matrix. The alignment of EAMR results with those obtained from SAW, TOPSIS methods reinforces the reliability of the proposed multi-criteria evaluation framework.

Table 9. Values of G_i^+, G_i^-, S_i, and ranking of alternatives using the EAMR method

Specimen	G_i^+	G_i^-	S_i	Rank
1	0.707725	0.171742	4.120868	2
2	0.80573	0.190782	4.223294	1
3	0.660493	0.171299	3.855783	3
4	0.687935	0.19399	3.546238	6
5	0.480267	0.171371	2.802495	8
6	0.677621	0.187801	3.608193	5
7	0.63267	0.167718	3.772225	4
8	0.562515	0.190469	2.953316	7

4.5. COMPARATIVE DISCUSSION OF MCDM RESULTS

A comparative analysis of the three MCDM methods reveals a high level of consistency in ranking outcomes. Specimen 2 is unanimously identified as the optimal design across all applied methods, demonstrating the robustness and stability of the decision-making framework. This consistency indicates that the superior mechanical performance of Specimen 2 is not method-dependent but is intrinsically linked to its favourable combination of low mass, high load-bearing capacity, minimal deformation, and high elastic modulus.

The consistent identification of Specimen 2 as the top-ranked alternative across all applied MCDM methods can be attributed to a synergistic combination of its geometric configuration, material composition, and load-transfer efficiency.

Firstly, Specimen 2 exhibits the highest load-bearing capacity among all tested structures (18.54 kN), which is the most influential criterion according to the MEREC-based weighting analysis ($w_F = 0.4873$). This dominant contribution indicates that the mechanical robustness of Specimen 2 plays a decisive role in the overall ranking. The enhanced load-bearing performance suggests that its internal architecture provides efficient stress redistribution and minimizes localized stress concentrations under compressive loading.

Secondly, Specimen 2 achieves the highest elastic modulus (707.26 MPa), ranking first among all specimens. Given the substantial weight assigned to elastic modulus ($w_E = 0.3105$), this characteristic significantly reinforces the structural stiffness of Specimen 2 and contributes to its superior performance in deformation-sensitive applications. The combination of high stiffness and load-bearing capacity implies a mechanically stable structure capable of sustaining high compressive loads with limited elastic deformation.

Thirdly, although Specimen 2 does not exhibit the minimum mass or deformation, its values remain within a competitive and acceptable range compared to other specimens. Importantly, the relatively lower weights assigned to mass ($w_m = 0.0656$) and deformation ($w_\varepsilon = 0.1367$) indicate that moderate trade-offs in these criteria do not significantly penalize the overall ranking. This highlights that Specimen 2 achieves an optimal balance between lightweight characteristics and mechanical strength rather than excelling in a single isolated metric.

From a structural perspective, the superior performance of Specimen 2 can also be explained by its optimized bio-inspired geometry combined with carbon fiber reinforcement (PLA–CF). The presence of short carbon fibers enhances stiffness and load transfer within the polymer matrix, while the continuous and well-connected internal architecture facilitates uniform stress distribution and delays the onset of structural instability. This synergy between material reinforcement and geometric efficiency leads to improved mechanical performance compared to non-reinforced or less optimized structures.

Finally, the high consistency of ranking outcomes across multiple MCDM techniques confirms that the optimality of Specimen 2 is not method-dependent but is instead a robust consequence of its experimentally measured mechanical properties. This convergence provides strong evidence that Specimen 2 represents the most mechanically efficient design among the investigated alternatives under the selected multi-objective criteria. Overall, the convergence of results obtained from SAW, TOPSIS, EAMR methods provides strong evidence for the effectiveness of integrating objective weighting (MEREC) with multiple MCDM techniques in the optimization of bio-inspired FDM-printed structures. To further verify ranking stability, a sensitivity analysis was conducted by perturbing each MEREC weight by ±10% while renormalizing the remaining weights.

The top-ranked alternative (Specimen 2) remained unchanged in all perturbation scenarios for SAW, TOPSIS, and EAMR. In addition, Spearman rank correlations between methods were above 0.9, confirming strong agreement and robustness of the decision outcome. Compared to previous MCDM studies in additive manufacturing, which typically rely on a single method with subjective weighting, the present work integrates objective weighting (MEREC) with multiple ranking techniques, reducing bias and improving decision reliability. While most existing studies focus on process parameters or material selection, this work extends MCDM to TPMS-based architected structures using experimentally validated

mechanical data, providing a more practical evaluation framework. In summary, the strong agreement among methods, supported by sensitivity analysis and rank correlation, confirms the robustness of the proposed approach and indicates that the optimal design is not method-dependent but governed by its intrinsic mechanical performance.

5. CONCLUSION

This study presented a systematic and experimentally validated framework for the multi-objective optimization of mechanical performance in bio-inspired structures fabricated by fused deposition modelling (FDM). Four representative bio-inspired geometries, Gyroid (G), I-graph-wrapped package (IWP), Fischer–Koch–S (FKS), and Primitive–Gyroid–Modified–Y (PMY), were designed using implicit level-set formulations and fabricated using PLA and PLA reinforced with short carbon fibers (PLA–CF). Compression experiments were conducted to evaluate mass, deformation, load-bearing capacity, and elastic modulus, providing reliable experimental data for multi-criteria decision-making (MCDM) analysis.

An objective weighting scheme based on the MEREC method was employed to quantify the relative importance of the selected criteria, revealing that load-bearing capacity and elastic modulus are the most influential factors governing overall performance. Three complementary MCDM techniques, SAW, TOPSIS, and EAMR, were subsequently applied to rank the candidate structures. The high consistency of ranking results across the three MCDM methods confirms the robustness and reliability of the proposed optimization framework.

Among the investigated alternatives, Specimen 2 (PMY geometry fabricated using PLA–CF) was consistently identified as the optimal design. This specimen exhibits a favourable balance of low mass, high load-bearing capacity, minimal deformation, and superior elastic modulus. Its superior performance is attributed to the synergistic effects of bio-inspired hybrid geometry and carbon fiber reinforcement, which collectively enhance stress redistribution, stiffness, and structural stability under compressive loading.

The findings of this study demonstrate that integrating bio-inspired structural design with objective MCDM-based optimization provides a powerful tool for the rational design of mechanically efficient additively manufactured structures. The proposed framework is general and can be readily extended to other materials, geometries, and additive manufacturing processes. Future work will focus on incorporating additional performance criteria, such as energy absorption, fatigue resistance, and multi-axial loading behaviour, as well as extending the framework to multi-scale optimization and machine learning-assisted design. These advancements are expected to further enhance the applicability of bio-inspired structures in advanced engineering applications.

ACKNOWLEDGEMENTS

This research was funded by the Vietnam Ministry of Education and Training, grant number B2024-TNA-21.

REFERENCES

[1] NGO T.D., KASHANI A., IMBALZANO G., NGUYEN K.T.Q., HUI D., 2017, *Additive Manufacturing (3D Printing): a Review of Materials , Methods , Applications and Challenges*, Compos. Part B, 143, December, 172–196.

[2] MAZURCHEVICI A.D., NEDELCU D., POPA R., 2020, *Additive Manufacturing of Composite Materials by FDM Technology: A Review*, Indian J. Eng. & Mater. Sci., 27, April, 179–192.

[3] HO T.N.-T., NGUYEN S.H., LE V.T., HOANG T.-D., 2024, *Coupling Design and Fabrication of Continuous Carbon Fiber-Reinforced Composite Structures Using Two-Material Topology Optimization and Additive Manufacturing*, Int. J. Adv. Manuf. Technol., 130/9, 4277–4293.

[4] SAROIA J., et al., 2020, *A Review on 3D Printed Matrix Polymer Composites: Its Potential and Future Challenges*, Int. J. Adv. Manuf. Technol., 106/5–6, 1695–1721.

[5] GUPTA A., BABU S.L., 2023, *Triply Periodic Minimal Surfaces: An Overview Of Their Features, Failure Mechanisms, and Applications*, J. Mines, Met. Fuels, 70, 211–221.

[6] WAKJIRA Y., CIONI A., LEMU H.G., 2024, *Current Status of the Application of Additive-Manufactured TPMS Structure in Bone Tissue Engineering*, Prog. Addit. Manuf., 0123456789.

[7] HOANG T.-D., NGO T.H., TRAN K.Q., LI S., NGUYEN-XUAN H., 2025, *A Stochastic Multiscale Asymptotic Homogenization Approach to 3D Printed Biodegradable Resin TPMS Bio-Inspired Structures*, Thin-Walled Struct., 212, 113100.

[8] HASSAN I.M., ENAB T.A., FOUDA N., ELDESOUKY I., 2023, *The Mechanical Performance of Functionally Graded Schwarz Primitive and Schoen-IWP Cellular Structures Fabricated by Additive Manufacturing*, Prog. Addit. Manuf., 8/2, 303–311.

[9] FENG J., FU J., YAO X., HE Y., 2022, *Triply Periodic Minimal Surface (TPMS) Porous Structures: from Multi-Scale Design, Precise Additive Manufacturing to Multidisciplinary Applications*, Int. J. Extrem. Manuf., 4/2.

[10] SATHISHKUMAR N., ARUNKUMAR N., ROHITH S.V., HARIHARAN R.R., 2023, *Publisher Correction: Effect of Varying Unit Cell Size on Energy Absorption Behaviour of Additive Manufactured TPMS PETG Lattice Structure*, Prog. Addit. Manuf., 8/6, 1715.

[11] QIU N., WAN Y., SHEN Y., FANG J., 2024, *Experimental and Numerical Studies on Mechanical Properties of TPMS Structures*, Int. J. Mech. Sci., 261, January, 1–35.

[12] LI X., et al., 2024, *Enhanced Mechanical Properties of Sandwich Panels Via Integrated 3D Printing of Continuous Fiber Face Sheet and TPMS Core*, Thin-Walled Structures.

[13] LAL LAZAR P.J., SUBRAMANIAN J., NATARAJAN E., MARKANDAN K., RAMESH S., 2023, *Anisotropic Structure-Property Relations of FDM Printed Short Glass Fiber Reinforced Polyamide TPMS Structures Under Quasi-Static Compression*, J. Mater. Res. Technol., 24, June, 9562–9579.

[14] BREISH F., HAMM C., KIENZLER R., 2025, *Beyond Global Mechanical Properties: Bio-Inspired TPMS Cellular Solids for Efficient Mechanical Design and Optimization*, Adv. Eng. Mater., 27, 2402105.

[15] FORES-GARRIGA A., GOMEZ-GRAS G., PEREZ M.A., 2023, *Additively Manufactured Three-Dimensional Lightweight Cellular Solids: Experimental and Numerical Analysis*, Mater. Des., 226, February.

[16] EMOVON I., OGHENENYEROVWHO O.S., 2020, *Application of MCDM Method in Material Selection for Optimal Design: A Review*, Results Mater., 7, 100115.

[17] CIARDIELLO F., GENOVESE A., 2023, *A Comparison Between TOPSIS and SAW Methods*, Ann. Oper. Res., 325/2, 967–994.

[18] WANG P., ZHU Z., WANG Y., 2016, *A Novel Hybrid MCDM Model Combining the SAW, TOPSIS and GRA Methods Based on Experimental Design*, Inf. Sci. (Ny)., 345, 27–45.

[19] SOUAIDI C., YALLESE M.A., AMIRAT A., BELHADI S., MABROUKI T., 2024, *Analysis, Modelling and Optimization During Sustainable Dry and MQL Turning of AISI 52100 Steel Using DF, GRA, EAMR, EDAS and FUCA Methods*, Int. J. Adv. Manuf. Technol., 135, 11, 5035–5069.

[20] KUMAR S., AHIJITH KUMAR P.V., BHARATI K., PATNAIK L., RANJAN MAITY S., LEPICKA M., *Coating Material Selection for Bulk Metal Forming Dies: a MEREC-Integrated Approach with Multiple MCDM Methods*, Int. J. Interact. Des. Manuf., 19/6, 4055–4070.